Mobility-Aware Coordinated Charging for Electric Vehicles in VANET-Enhanced Smart Grid

Miao Wang, *Student Member, IEEE*, Hao Liang, *Member, IEEE*, Ran Zhang, *Student Member, IEEE*, Ruilong Deng, *Student Member, IEEE*, and Xuemin Shen, *Fellow, IEEE*

***Abstract*—Coordinated charging can provide efficient charging plans for electric vehicles (EVs) to improve the overall energy utilization while preventing an electric power system from overloading. However, designing an efficient coordinated charging strategy to route mobile EVs to fast-charging stations for globally optimal energy utilization is very challenging. In this paper, we investigate a special smart grid with enhanced communication capabilities, i.e., a VANET-enhanced smart grid. It exploits vehicular ad-hoc networks (VANETs) to support real-time communications among road-side units (RSUs) and highly mobile EVs for collecting real-time vehicle mobility information or dispatching charging decisions. Then, we propose a mobility-aware coordinated charging strategy for EVs, which not only improves the overall energy utilization while avoiding power system overloading, but also addresses the range anxieties of individual EVs by reducing the average travel cost. Specifically, the mobility-incurred travel cost for an EV is considered in two aspects: 1) the travel distance from the current position of the EV to a charging station; and 2) the transmission delay for receiving a charging decision via VANETs. The optimal mobility-aware coordinated EV charging problem is formulated as a time-coupled mixed-integer linear programming problem. By solving this problem based on Lagrange duality and branch-and-bound-based outer approximation techniques, an efficient charging strategy is obtained. To evaluate the performance of the proposed strategy, a realistic suburban scenario is developed in VISSIM to track vehicle mobility through the generated simulation traces, based on which the travel cost of each EV can be accurately calculated. Extensive simulation results demonstrate that the proposed strategy considerably outperforms the traditional EV charging strategy without VANETs on the metrics of the overall energy utilization, the average EV travel cost, and the number of successfully charged EVs.**

***Index Terms*—Mobile EVs, coordinated fast charging, range anxiety, VANETs, smart grid.**

I. Introduction

ELECTRIC VEHICLEs (EVs), as a promising component of sustainable and eco-friendly transportation systems, have received considerable attention in many countries across the world [1], [2]. Refueled by electricity instead of gasoline, these vehicles have the potential to save thousands of dollars for customers over the vehicle lifetime. For example, a TESLA Model S, a pioneer retail EV produced by TESLA Motors, costs $30/km, while a common premium sedan costs $173/km [3]. Besides, the adoption of EVs into the transport sector can reduce the consumption of conventional energy sources (e.g., gasoline) and the pollution of environments (e.g., greenhouse gas emissions). As reported in [4], battery EVs, which completely depend on rechargeable batteries and thus produce no emissions, can cut down the overall emissions from the transport sector by 70%. Due to the above advantages, EVs have been accounting for higher market share in the transport sector. According to the report of Electric Power Research Institute (EPRI) [5], the EV penetration level can reach 35%, 51%, and 62% by 2020, 2030, and 2050, respectively.

However, the widespread adoption of EVs in the transportation system will lead to charging problems of mobile EVs that are fully reliant on rechargeable batteries. EV charging, which is very likely to coincide concentratively with the peak demand time of the power system, can incur overloading of a distribution feeder, resulting in the system instability and the reduction in energy utilization [6], [7], especially for fast EV charging as it requires much higher power than the regular charging. Some works use energy storage systems to mitigate the impact of fast EV charging on the power system, but at an additional cost of deploying the energy storage devices [2]. Thus, to avoid power system overload during the peak time and improve energy utilization without additional deployment cost, load management strategies are indispensable to distribute the EV charging load both temporally and spatially in a coordinated fashion. At the same time, for fast EV charging, the assigned charging stations must be within the range of individual mobile EVs given current locations and battery energy levels, due to the tension between the current battery energy levels and the travel cost to reach charging stations, i.e., range anxiety.

There has been abundant literature [8]–[19] concerning the coordinated EV charging strategy design for EVs. But most of the works so far solve problems only in the power system aspect. That is, the coordinated charging is performed for a group of EVs that are assumed to be ready for charging within an area (e.g., parking lots or residence areas). Little research has considered vehicle-specific features, i.e. the vehicle mobility, into the charging strategy when fast-charging is considered. In fact, as EVs may need charging when moving on the road, the energy consumption on the road to reach the charging station, referred to as the travel cost in this paper, should be considered. Otherwise, the charging station assigned by the existing

Manuscript received March 27, 2014; accepted May 10, 2014. Date of publication June 19, 2014; date of current version August 13, 2014. This work was presented in part at the IEEE Globecom 2013.

M. Wang, H. Liang, R. Zhang, and X. Shen are with the Department of Electrical and Computer Engineering, University of Waterloo, Waterloo, ON N2L 3G1, Canada (e-mail: m59wang@uwaterloo.ca; h8liang@uwaterloo.ca; r62zhang@uwaterloo.ca; sshen@uwaterloo.ca).

R. Deng is with the Department of Control Science and Engineering, Zhejiang University, Hangzhou 310027, China (e-mail: dengruilong@zju.edu.cn).

Color versions of one or more of the figures in this paper are available online at http://ieeexplore.ieee.org.

Digital Object Identifier 10.1109/JSAC.2014.2332078

strategies may be too far to reach given the EV's current location and battery energy level. Due to this range anxiety, drivers prefer to charge at locations with less travel cost. Therefore, new charging strategies are required to take the range anxieties and vehicle mobility into consideration to reduce the EV travel cost. In order to track the vehicle mobility, real-time information of EVs (e.g., locations and battery energy levels) should be collected to assist charging strategy design.

To this end, in this paper, we focus on leveraging the real-time mobile vehicle information to help designing an efficient coordinated EV charging strategy. The objective is to improve the overall energy utilization, reduce the average EV travel cost, and prevent the overload of the power system. To properly design the strategy, two underlying key problems should be deliberated: 1) how to efficiently and reliably obtain the real-time information of mobile vehicles required by the EV charging strategy; and 2) based on the collected information, how to perform mobility-aware coordinated EV charging to improve energy utilization and reduce EV travel cost while avoiding power system overload.

Thanks to vehicular ad-hoc networks (VANETs), the first problem can have a promising resolution. Exclusively designed for information exchange among highly mobile vehicles and road-side units (i.e., RSUs) in a multi-hop fashion, VANETs can deliver the required real-time information efficiently via short-range vehicle-to-vehicle (V2V) and vehicle-to-RSU (V2R) communication [20]–[22], making large-volume vehicle information collection cheaper and faster compared to the other networks (e.g., cellular networks and Wi-Fis) [23]. More importantly, RSUs in VANETs can greatly enhance the timeliness of data collection and dissemination, which makes it possible to perform coordinated charging strategies for a group of moving vehicles [24]. Therefore, in this work, VANETs are integrated into a smart grid to collect the real-time information of mobile EVs and disseminate the charging decisions. Moreover, as the running EVs still consume energy when waiting for the charging decision, the transmission delay for information exchange in VANETs may cause additional travel cost for EVs. Thus in this paper, the transmission delay is analyzed based on the RSU deployment and vehicle densities.

To cope with the second problem, in this work, based on the VANET-enhanced smart grid, the range anxieties are considered based on vehicle mobility in the charging strategy design. Specifically, we propose a mobility-aware coordinated EV charging strategy to make charging decisions based on the collected real-time vehicle information and the historic remote terminal unit (RTU) readings of the power grid. With all the collected information, the following questions are answered in a coordinated fashion: 1) should a vehicle be charged in the next period based on current battery energy level; 2) which charging station should this vehicle go to with the consideration of the range anxiety based on its current location; and 3) how much energy should be charged for this vehicle to improve the energy utilization and guarantee the power system stability. The optimal charging problem is formulated as a time-coupled mixed-integer linear programming (MILP) problem, which is difficult to be solved. However, by unveiling the linear relationship among EV charging loads of feeders, we decouple the MILP problem into a series of sub-MILPs through Lagrange duality [25]. Each sub-MILP can be further solved by the branch-and-cut-based outer approximation algorithm [26].

In summary, to deal with the range anxieties of EVs, we incorporate VANETs into the smart grid to collect real-time vehicle information for tracking the vehicle mobility (e.g., locations) and battery energy levels. A predictive mobility-aware coordinated EV charging strategy is proposed to improve the power utilization and reduce average EV travel cost while preventing overload of the power system for the following charging period. The main contributions of the paper are listed as fourfold.

- First, we propose the system architecture of the VANET-enhanced smart grid, in which VANETs enable efficient communication among mobile vehicles and RSUs to collect useful information and dispatch the decisions of the EV charging strategy in a real-time manner; a traffic server is in charge of processing the collected information and performing the predictive coordinated EV charging strategy for EVs;
- Second, considering the range anxieties of EVs, we design a mobility-aware coordinated EV charging strategy to improve the overall energy utilization of the power system and reduce the average EV travel cost while avoiding the overload of the power system. Particularly, we discover that the EV charging loads of charging stations present a linear relation, which is critical for the load assignment; furthermore, the travel cost is defined and formulated to reveal the impact of vehicle mobility on the charging strategy design;
- Third, the globally optimal charging problem is formulated as a time-coupled MILP problem which is decoupled into a series of sub-MILPs through Lagrange duality. Each sub-MILP is further solved by the branch-and-cut-based outer approximation algorithm; and
- Finally, we carry out extensive simulations to validate the effectiveness and efficiency of our proposed EV charging strategy. The simulation traces are extracted from VISSIM [27], by which a highly realistic suburban scenario is built. And the transmission delay induced by VANETs is fully evaluated. Then, the proposed strategy is demonstrated to considerably outperform the traditional autonomous charging strategy (without VANETs) on the metrics of the energy utilization and the average EV travel cost.

The remainder of this paper is organized as follows. The related work is discussed in Section II. Section III provides an overview of the system model. In Sections IV and V, the mobility-aware coordinated EV charging problem is formulated and solved, respectively. Section VI demonstrates the performance of the proposed strategy by simulations. Section VII concludes this paper.

II. Related Work

Up to now, many studies have shown that the power system can be significantly affected by high penetration levels of EV

charging [11], [12]. To avoid power system overloading during the peak time, load management strategies are indispensable to distribute the EV charging load both temporally and spatially [13]. In [14], [15], to avoid power system overloading, the peak load is shifted to off-peak periods to improve the load factor of the entire grid. In [16], [17], it is shown that global EV charging strategies that coordinate the charging duration and rates of multiple EVs based on global load information have better performance than the local strategy. In [18], [19], the spatial diversity of EV charging is modeled and evaluated to further help regulate the charging profile. However, most of the existing EV charging strategies consider EVs to be stationary when they need to be charged; few works take the vehicle mobility into consideration, which can not be overlooked as it is the most important feature of a vehicle, especially for fast-charging. Due to vehicle mobility, range anxiety, i.e., the tension between the travel cost and the EV battery energy level, is key to the viability of charging decisions. Therefore, new efficient EV charging strategies must be designed to take care of real-time vehicle information to solve the range anxiety problem.

To obtain the real-time vehicular information, most existing works rely on cellular or Wi-Fi systems [28]–[30]. However, inevitable drawbacks of these systems limit their practicability in the collection of vehicle information. First, for dense vehicular networks, the inaccuracy of the location measurement in both systems [31] may considerably degrade the charging performance. Second, as cellular systems are not dedicated for vehicular data collection, the collection services can be highly costly, and the high volume of vehicular data may cause congestion for other cellular services especially when the vehicle density is high; for the Wi-Fi systems, the coverage is very limited which can cause large delay in information delivery, and the high mobility of vehicles may dramatically reduce the delivery ratio. Thanks to VANETs, the delivery of the real-time message can be much quicker, cheaper and more efficient than the above systems, especially for dense and highly mobile vehicular networks [32]. Exclusively designed for information exchange among highly mobile vehicles and the RSUs, the supported short-range V2V and V2R communication effectively expands the transmission range of vehicles in a multi-hop manner with higher data rates. As a result of the RSU sharing and multiple V2V relaying mechanisms, a higher throughput and delivery ratio as well as lower delay can be achieved for the large-volume vehicle information exchange [33], [34], making it possible to perform coordinated charging strategy for a group of vehicles. In this paper, we exploit VANETs in a smart grid to support the real-time information exchange among mobile vehicles, and evaluate the transmission delay possibly incurred by VANETs. Then, the range anxiety which describes the tension between the travel cost and the current energy level can be introduced as a viability of the charging decisions for mobile vehicles.

Therefore, with real-time vehicle information collection and decision dissemination through VANETs, our objective is to design a mobility-aware coordinated predictive charging strategy for mobile EVs. This strategy improves the energy utilization of the power system and reduces the average EV travel cost while avoiding overload in the power system.

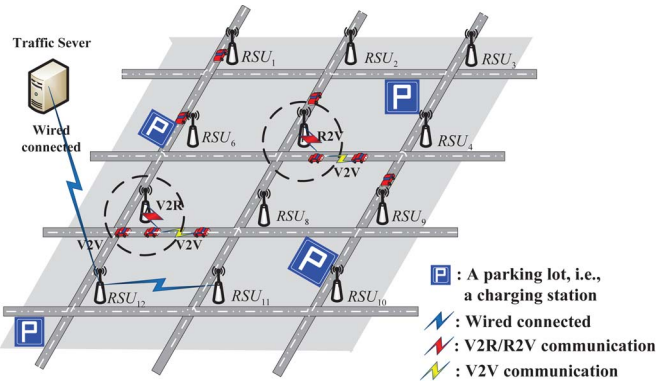

Fig. 1. The VANET-enhanced smart grid architecture.

III. System Model

Aiming at providing a predictive coordinated mobility-aware charging strategy for EVs based on the real-time vehicle information, we first introduce a VANET-enhanced smart grid architecture to efficiently operate the coordinated EV-charging strategy. Then, the power flow equations are elaborated in the corresponding power system. Furthermore, the mobility model, charging model and transmission model of EVs are discussed.

A. VANET-Enhanced Smart Grid

Fig. 1 shows the components of the proposed VANET-enhanced smart grid architecture, consisting of a power distribution system, charging stations (e.g., at parking lots), a traffic server, EVs and access points (i.e., RSUs) along road sides. The power distribution system supplies energy to the whole network through power feeders (i.e., buses). Besides, the charging stations provide fast-charging for all the EVs.

Based on historic RTU readings of each distribution system bus, the voltage at each charging station in the following period can be obtained [35]. The maximal power that can be supplied by each charging station (i.e., the load-capacity of each charging station) is preknown. In the following context, we denote the load-capacity of Bus_j as P^j_{total}. The historic readings are delivered to the traffic server via wireline. A traffic server is capable of performing predictive charging strategy to provide globally optimized charging decisions for EVs, according to the real-time EV information collected through VANETs and the historic RTU readings. The operation is conducted period by period. Specifically, the charging decisions include the charging load/rate of EV v at Bus_j in period k (denoted as $Pch_{v,j,k}$) and the charging indicator of vehicle v indicating whether EV v will be charged at station j in period k, which is denoted as $x_{v,j,k}$. And $x_{v,j,k}$ is set to 1 when EV v is charged at Bus_j in period k, and 0 otherwise.

In VANETs, consider a set of EVs, denoted as $\mathbb{V}$, moving around in the network region following map-based paths. EVs may need to be charged while moving on their ways. The real-time EV information can be exchanged among the on-board units (OBUs) installed in vehicles, through multi-hop

V2V relaying, based on dedicated-short-range-communication (DSRC) protocol [36],[1] with a transmission range R. Besides, Global Position System (GPS) devices, which offer the service of shortest-path navigation, are also equipped in EVs and keep wired connection with the OBU. Furthermore, a set of RSUs, denoted as $\mathbb{R}$, are uniformly deployed along roads and capable to collect the vehicle information (e.g., locations and battery energy levels) of EVs through V2R transmissions, based on DSRC protocol, with the transmission range R. Wiredly connected to the traffic server, RSUs can relay the collected vehicle information to the traffic server for calculating the globally optimized charging strategies for EVs. Thereafter, if RSUs obtain the EV charging decisions from the traffic server, they can relay the charging decisions to the EVs through R2V and V2V transmissions.

In summary, the VANET-enhanced smart grid system operates as follows.

- Information collection and delivery to the traffic server: The requested information are two-fold, i.e., the historic RTU readings of each bus in the power system and the real-time vehicle information. The former is delivered to the traffic server through wireline, based on which the charging load constraints of charging stations can be predicted; the latter is collected through multi-hop V2V relaying and V2R transmission;
- Decision making of the predictive coordinated EV charging: The traffic server then fuses all the collected information and calculates the optimal EV charging strategy to improve the power utilization of the grid and reduce the average EV travel cost while avoiding power system overloading;
- Decision dissemination: As soon as the OBU of an EV receives its own charging decision from either the neighboring EVs or an RSU, it will deliver the decision to the GPS, and the GPS will navigate that EV to the designated charging station.

B. Power System Model

In order to implement charging control for EVs in the VANET-enhanced smart grid, the power flow on the feeders should be considered. In the following, a power system model is described, where the relationship between bus voltages and loads are given to help derive the relation among EV charging loads of feeders.

Consider a smart grid based on the system model as shown in Fig. 1. The power system can be abstracted as a one-line diagram with multiple buses. For further illustration, an example of a 12-bus system is depicted in Fig. 2(a). And Fig. 2(b) is the equivalent power system model of Fig. 2(a). Let N denote the set of buses in the system, with the population of 12 in this example. The *generation buses* are defined as the buses injecting power to the system, i.e., Bus_1 in Fig. 2(a), while the others which only have load are denoted as the *load buses*, i.e., Bus_3, Bus_6, etc. The power system is supplied through

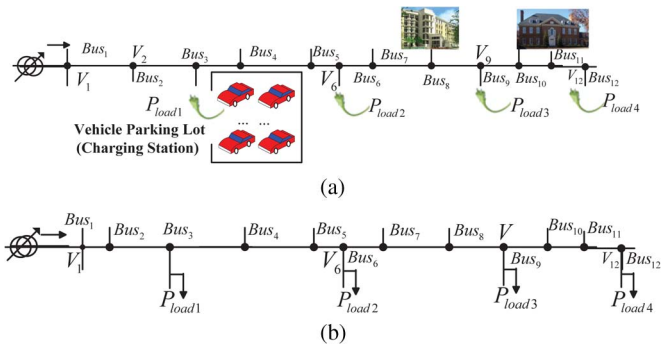

Fig. 2. The power system model. (a) Illustrated power system model. (b) Equivalent power system.

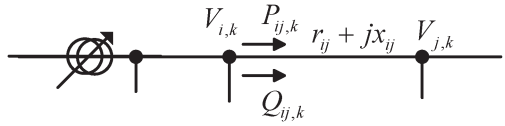

Fig. 3. The power flow illustration.

the substation at the generation bus, i.e., Bus_1. EV charging stations are located in the network at load buses, e.g., Bus_3, Bus_6, Bus_9, and Bus_{12}, respectively. Consider that each charging station is connected to the grid via a standard single-phase Alternating-Current (AC) connection. Due to the thermal limit of service cable or current rating of fuse, an EV charging station at Bus_j is subject to a load-capacity constraint P^j_{total} [15]. Although the concept of vehicle-to-grid for a local system exists [8], bi-directional flow of electricity or the directional flow from an EV battery is not considered in this work.

The voltages of two neighboring buses in period k, e.g., $V_{i,k}$ and $V_{j,k}$ as depicted in Fig. 3, can be approximated as [35]

$$V_{i,k} - V_{j,k} = \frac{P_{ij,k} \cdot r_{ij} + Q_{ij,k} \cdot x_{ij}}{V_{j,k}} \tag{1}$$

where $P_{ij,k}$ and $Q_{ij,k}$ are the active and reactive power flow from Bus_i to Bus_j in period k, respectively, while $r_{ij} + jx_{ij}$ is the impedance of the feeder line $i - j$. In per unit, (1) is usually approximated as

$$V_{i,k} - V_{j,k} = P_{ij,k} \cdot r_{ij} + Q_{ij,k} \cdot x_{ij}. \tag{2}$$

Note that all the voltages of buses should be within a certain range which is the main constraint of distribution system operation [35]. Specifically, the voltage magnitude at Bus_j in period k is bounded by the upper and lower limits $V^{\min}_{j,k}$ and $V^{\max}_{j,k}$, respectively, i.e., $V^{\min}_{j,k} \le V_{j,k} \le V^{\max}_{j,k}$. As proved in [35], the minimum voltage point can occur only at the end of the feeder, since only one generation bus is located at the beginning of the distribution system.[2] The minimum voltage $V_{N,k}$ can be calculated as

$$V_{N,k} = V_{1,k} - \sum_{i=1}^{N-1} \left[P_{i(i+1),k} \cdot r_{i(i+1)} + Q_{i(i+1),k} \cdot x_{i(i+1)} \right]. \tag{3}$$

[1]DSRC protocol supports both RSU-to-vehicle/vehicle-to-RSU (R2V/V2R) and vehicle-to-vehicle (V2V) communication.

[2]Note that if the distributed generation is adopted in the distribution system, the overloading problem should also be considered.

C. EV Mobility and Charging Model

Consider that EVs move along the roads in the studied area. The mobility of each EV can be characterized by two random variables (V, D) [37]. Here, V represents the vehicle velocity which takes two possible values (i.e., a lower velocity v_L and a higher velocity v_H). The velocity transition is modeled as a two-state continuous Markov chain with state transition rate $1/D$. Under this model, a vehicle initially chooses v_L (or v_H), and after a time interval which is exponentially distributed with the mean of D, the velocity changes to v_H (or v_L). The model can be exploited to describe the realistic driving behaviors of people, i.e., a driver usually drives at a constant velocity for a period and then changes to a higher/lower velocity based on his/her will or road conditions. Besides, when the vehicle density is low or medium (e.g, when the vehicle density is no larger than 30 vehicle/km/lane), vehicles can be considered to move independently [38] and the headway distance[3] follows the exponential distribution with rate ζ [39].

When a mobile EV needs to be charged, the charging load of EV $v(\in \mathbb{V})$ at Bus_j in period k, i.e., $Pch_{v,j,k}$, should be within a certain range, i.e.,

$$0 \leq Pch_{v,j,k} \leq Pch^{\max}_{v,j,k} \tag{4}$$

where $Pch^{\max}_{v,j,k}$ is the predefined charging load bound of $Pch_{v,j,k}$ [40]. If EV v is not planned to be charged in period k, i.e., $x_{v,j,k} = 0$, the charging load of EV v in period k should be 0, i.e.,

$$\frac{Pch_{v,j,k}}{Pch^{\max}_{v,j,k}} \leq x_{v,j,k} \tag{5}$$

Also, $x_{v,j,k}$ should satisfy

$$\sum_{j\in H} x_{v,j,k} \leq 1 \text{ and } x_{v,j,k} \in X = [0,1] \cap \mathbb{Z}$$

$$\sum_{k}\sum_{j\in H} x_{v,j,k} \leq X_{\max} \tag{6}$$

where $X_{\max}$ is the upper bound of the total charging times for an EV within all the considered periods, since the frequently charging is not necessary for EVs and may result in battery damages [41]. For example, if each EV has at most three chances to be charged within all the considered periods, $X_{\max} = 3$. During a charging period, the charging energy of each EV should be limited by its battery-capacity $C^{\max}_{\text{battery}}$, and the battery should not be depleted on the way and failed to be charged, i.e.,

$$0 \leq P^{\text{init}}_{v,k} + \left(\sum_{j\in H} a \cdot Pch_{v,j,k} - P^{v,k}_{cost} - P^{k}_{\text{cons}} \cdot \left(1 - \sum_{j\in H} x_{v,j,k}\right)\right) \leq C^{\max}_{\text{battery}} \tag{7}$$

[3]In this paper, the headway distance is defined as the distance between two neighboring vehicles in the same lane.

where $P^{\text{init}}_{v,k}$ is the initial energy stored in EV v in period k obtained via VANETs, and $P^{v,k}_{cost}$ is the travel cost for charging in period k for EV v. Let P^{k}_{cons} be the average non-charging energy cost of each EV for moving on the road if the EV is not charged in period k. The duration of each period is a hours. For instance, if we consider a 30-minutes duration for each period, we have $a = 0.5$. Then, for an EV charging station at Bus_j, the total EV load $Pch_{j,k}$ in period k is

$$Pch_{j,k} = \sum_{v\in\mathbb{V}} Pch_{v,j,k}. \tag{8}$$

D. Transmission Model in VANETs

To support the V2V and V2R communication in VANETs, the draft standard IEEE 802.11p [42] (DSRC) is adopted, which is designed particularly for short-range and intermittent vehicle-based communications among vehicles and RSUs. For analytical simplicity, in the link layer, we consider ideal medium access control (MAC) protocol. Under ideal MAC, the interference among V2V transmissions can be avoided, and once one vehicle moves into the coverage range of an RSU, the RSU is capable to schedule time slots of V2R transmission for the vehicle with no collisions. Besides, the link data rate of a V2V or V2R transmission is considered to be constant, and the contact duration between each transmission pair (e.g., V2V or V2R) is considered long enough to accomplish one packet delivery, which can be achieved by appropriately setting the packet size [32]–[34]. Moreover, due to the intermittency of vehicle communications caused by high-speed mobility, the waiting time for obtaining a transmission opportunity is dominant in the transmission delay compared to the queueing delay and the random backoff time due to the channel contention. Therefore, only the former is considered in this paper.

IV. Problem Formulation

In this section, charging load constraints are first calculated for the buses with EV charging stations. And the relationship among the EV charging loads of buses are discovered. Then, considering the mobility of EVs, the EV's travel cost is formulated to represent the range anxieties of EVs, which particularly involves the cost induced by the transmission delay in VANETs. Finally, the mobility-aware coordinated EV charging problem is formulated to maximize the overall charging-energy-minus-travel-cost with power system overloading avoidance. This objective indicates that the total charging energy improvement and the charging travel cost reduction should be jointly considered and carefully balanced.

A. Charging Load Constraints

The charging station at Bus_j is subject to a load-capacity constraint P^{j}_{total}. Combining the load-capacity constraint with the total EV load at Bus_j in period k of (8), we have

$$Pch_{j,k} \leq P^{j}_{\text{total}}. \tag{9}$$

Moreover, subject to the additional load of EVs, the voltage of one bus will decrease with the increased load [35]. If a voltage sags out of the threshold at a bus, the reactive power cannot be correctly and efficiently injected. To keep the voltage within the certain range, it is indispensible to reduce the load. Therefore, there should exist a tradeoff between voltages and loads. In the following, we give the inherent relationship among the EV charging loads of buses in *Theorem 1*, and the proof is given based on power flow analysis in the power system.

Theorem 1—(Linear Relation Among EV Charging Loads of Buses): Given the total supplied power of the feeder and the power demand of non-EV charging load, the total power supply to all EV charging stations can be calculated; and the power supplied to an individual charging station has a *linear relation* with those to the other charging stations.

Proof: For all the buses, the voltages should be no less than the minimal required voltage, for example, 0.9 per unit voltage [15]. From (3), the lowest voltage is $V_{N,k}$ of Bus_N. Then,

$$V_{N,k} = V_{1,k} - \sum_{i=1}^{N-1} \left[P_{i(i+1),k} \cdot r_{i(i+1)} + Q_{i(i+1),k} \cdot x_{i(i+1)}\right] \geq V_{\min} \tag{10}$$

where $V_{\min}$ is the minimal required voltage. Rearranging (10), we have

$$\sum_{i=1}^{N-1} \left[P_{i(i+1),k} \cdot r_{i(i+1)} + Q_{i(i+1),k} \cdot x_{i(i+1)}\right] \leq V_{1,k} - V_{\min}. \tag{11}$$

Let w be the sorted index of the bus without EV charging load and W be the set of these buses $w \in W(\subset N)$; let j be the sorted index of the bus with EV charging load and H be the set of these buses $j \in H(\subset N)$. Then, (11) can be represented by

$$\sum_{w \in W} \left(P_{w(w+1),k} \cdot r_{w(w+1)} + Q_{w(w+1),k} \cdot x_{w(w+1)}\right) + \sum_{j \in H} j \cdot (P_{j,k} \cdot r_j + Q_{j,k} \cdot x_j) \leq V_{1,k} - V_{\min} \tag{12}$$

where $P_{j,k}$ and $Q_{j,k}$ are the active and reactive power load on Bus_j in period k, and $r_j = (1/j)\sum_{h=1}^{j-1} r_{h(h+1)}$ and $x_j = (1/j)\sum_{h=1}^{j-1} x_{h(h+1)}$ represent the average impedance of the feeder line among Bus_1 and Bus_j. Since the loads of the buses without EV loading are constant based on the forecast [43], [44], we have

$$\sum_{j \in H} j(P_{j,k} \cdot r_j + Q_{j,k} \cdot x_j) \leq V_{1,k} - V_{\min} - \sum_{w \in W} \left(P_{w(w+1),k} \cdot r_{w(w+1)} + Q_{w(w+1),k} \cdot x_{w(w+1)}\right). \tag{13}$$

Since each charging station is connected to the grid via a single-phase AC connection and EV charging only draws active power, we have $P_{j,k} = Pch_{j,k}$ and $Q_{j,k} = 0$. Therefore, (13) can be rewritten as

$$\sum_{j \in H} jPch_{j,k} \cdot r_j \leq \Xi \tag{14}$$

where Ξ is a constant representing the RHS of inequality (13). The inequality (14) implies that the total power supply to EV charging stations is related to the locations of charging stations and the total number of the charging stations. If the total power supply to EV charging stations, i.e., Ξ, is given, the total EV load of the charging station at Bus_j, $Pch_{j,k}$, in period k, presents a *linear relation* with the others. ■

B. Travel Cost for EV Charging

With the mobility model defined in Section III-C, the travel cost $P_{cost}^{v,k}$ for EV v to be charged in period k should consist of two parts. On one hand, moving EVs may have different locations and battery energy levels at different periods. Due to the range anxiety, drivers prefer closer charging stations with less travel distance. Thus the travel distance from EV v's current position to a charging station in period k, denoted as $p_{v,k}$, should be considered. On the other hand, the vehicle mobility will result in intermittent V2V and R2V connections, which can introduce a transmission delay and thus involve an additional travel distance until EV v receives the charging decision from the RSUs. Thus the travel cost caused by the transmission delay for EV v to receive a charging decision via VANETs, denoted as $c_{v,k}$, should also be considered.

1) Travel Cost Due to the EV Travel Distance to a Charging Station: If the charging strategy guides EV v to be charged in the next period k, then $\sum_{j \in H} x_{v,j,k} = 1$. The traveling path for EV v to the charging station j in period k is calculated by the deployed GPS based on the shortest path algorithm [45], whose path length is denoted as $S(x_{v,j,k})$. Thus, the travel distance of EV v in period k for charging is defined as

$$p_{v,k} = \sum_{j \in H} S(x_{v,j,k}) \cdot x_{v,j,k}. \tag{15}$$

Based on $p_{v,k}$, the travel cost for EV v in period k in terms of energy is denoted as $PC(p_{v,k})$, where $PC(\cdot)$ is a linear non-decreasing function to measure the impacts of travel distance on the travel cost [8].

2) Travel Cost Due to the Transmission Delay in VANETs: The other part of the travel cost comes from the transmission delay for an EV to send (receive) the charging request (decision) to (from) the nearest RSU, due to the vehicle intermittent connections in the vehicular network.

First, we evaluate the transmission delay for the last hop of an uplink (i.e., the last V2I hop); the transmission delay is mainly due to the inter-contact time between a vehicle and an RSU. Define the last hop as an "on-off" model [37] where the vehicle either directly connects to an RSU (i.e., during the "on" state) or is the only vehicle approaching the RSU and there is no other vehicles in the transmission range of the RSU (i.e., during the "off" state). Since during the "on" state, the transmission delay for a message-packet is way smaller than the delay in the "off"

state, the transmission delay is mainly due to the "off" period. Note that the period here is a random variable and is different from the charging period.

Denote the "on" period and the "off" period of a vehicle as T_{on} and T_{off}, respectively. Accordingly, the travel distances within the periods are defined as U_{on} and U_{off} respectively, with $T_{on} = U_{on}/\overline{V}$ and $T_{off} = U_{off}/\overline{V}$. Here, $\overline{V}$ is the average velocity for a vehicle based on the "on-off" mobility model as defined in Section III-C. Similar to [37], the event that a vehicle moves a distance of at least u during T_{on} before being scheduled to communicate with RSU should satisfy that 1) there are no other vehicles within the distance u, and 2) there is at least one vehicle within the distance $2R-u$ which results in this vehicle moving at least u distance to avoid the collision, where R is the transmission range of both an RSU and a vehicle. Then, we have

$$P_r(U_{on} > u) = \frac{\left(e^{-\zeta\cdot u}\right)^{b\Gamma-1}\left[1-\left(e^{-\zeta\cdot(2R-u)}\right)^{b\Gamma-1}\right]}{1-\left(e^{-\zeta\cdot 2R}\right)^{b\Gamma}} \quad (16)$$

where b is the total length of roads, while Γ is the vehicle density on the roads. Since the vehicle headway distance follows an exponential distribution as mentioned in Section III-C, the probability that a headway distance is larger than u is $e^{-\zeta\cdot u}$. And

$$E(U_{on}) = \int_0^{2R} P_r(U_{on} > u)\, du. \quad (17)$$

Similarly, the event that a vehicle moves a distance of at least u during T_{off} should satisfy that 1) there are no vehicles within a distance of $2R+u$ from the end of the coverage range of the nearest RSU ahead the vehicle, and 2) there is at least one vehicle within the distance $L-(u+2R)$, where L is the distance between the adjacent RSUs. Then, we have

$$P_r(U_{off} > u) = \frac{\left(e^{-\zeta\cdot(2R+u)}\right)^{b\Gamma-1}\left[1-\left(e^{-\zeta\cdot(L-(2R+u))}\right)^{b\Gamma-1}\right]}{\left(e^{-\zeta\cdot 2R}\right)^{b\Gamma}\left[1-\left(e^{-\zeta\cdot(L-2R)}\right)^{b\Gamma}\right]} \quad (18)$$

$$E(U_{off}) = \int_0^{L-2R} P_r(U_{off} > u)\, du. \quad (19)$$

In addition, the previous hops within a communication link except the last hop are based on V2V communications which can be characterized with the mobility model of vehicles. The process of the relative velocity between two vehicles can be represented by a continuous time Markov chain (CTMC) with a state space $\mathbb{H} = \{h_0, h_1, h_2\}$. Here, h_0 represents a negative relative velocity when the vehicle in front moves with v_L while the vehicle behind moves with v_H; h_1 models a zero relative velocity (i.e., both vehicles move with the same velocity); h_2 represents a positive relative velocity. If each vehicle keeps the same velocity for an exponential time with an average time of D, the transition rate between any two states of the Markov process equals to $2/D$. Thus, from [37], the average number of hops M within a communication link can be approximated as

$$M = \frac{6\left(L - E[U_{on}] - E[U_{off}]\right)}{D(v_L + v_H)}. \quad (20)$$

Then, based on the average number of hops, the transmission delay of a uplink can be shown as

$$\psi = (M-1)E[T_{V2V}] + E[T_{off}] \quad (21)$$

where $E[T_{V2V}]$ is the average transmission delay for a V2V hop. And $E[T_{V2V}] = 1/(1-e^{\zeta R})$ with the vehicle transmission range R, since the headway distance follows exponential distribution. If we consider the downloading as a similar process with uploading, the total transmission delay should be 2ψ. Note that this transmission delay is related to the parameters in the network, e.g., vehicle mobility parameters (i.e., v_L, v_H, ζ, and D), the vehicle density (i.e., Γ), and the RSU deployment in the network (i.e., the transmission range R and the average distance between RSUs L).

Therefore, the average travel distance, $c_{v,k}$, during which EV v is moving and waiting for the charging decision in period k, can be calculated as

$$c_{v,k} = E[O_v] \cdot \sum_{j\in H} x_{v,j,k} \quad (22)$$

where $O_v = \overline{V}\cdot 2\psi(v_L, v_H, D, \zeta, \Gamma, R, L)$ is defined as the travel distance for EV v due to the transmission delay. Similarly, the travel cost due to the transmission delay is denoted as a linear non-decreasing function $PC(c_{v,k})$ to measure the energy cost for EV v to wait for receiving the decision in period k. With the defined $PC(p_{v,k})$ and $PC(c_{v,k})$, the current stored energy, $P_{v,k}^{\text{init}}$, should be no less than the summation of $PC(p_{v,k})$ and $PC(c_{v,k})$; otherwise, the battery will be depleted before the EV reaching the destination,

$$P_{cost}^{v,k} = PC(p_{v,k}) + PC(c_{v,k}) \le P_{v,k}^{\text{init}}. \quad (23)$$

Note that $P_{v,k}^{\text{init}}$ can be real-time collected by RSUs based on V2V and V2I communications.

C. Mobility-Aware EV Charging Optimization Problem

Taking account of both the EV charging load relationship among charging stations and the travel cost for EVs, the objective of the charging strategy is to maximize the overall charging-energy-minus-travel-cost with power system overloading avoidance [25]. This objective indicates that the total charging energy improvement and the charging travel cost reduction should be jointly considered and carefully balanced. Specifically, once the traffic server receives 1) the historic information from the RTUs located at the buses, and 2) the vehicle information via VANETs, a charging strategy is calculated to

determine $Pch_{v,j,k}$ and $x_{v,j,k}$, according to the optimization problem shown as follows.

$$\begin{aligned}
&\max \sum_k \sum_{v\in\mathbb{V}} \sum_{j\in H} a \cdot Pch_{v,j,k} \\
&\quad - \sum_k \sum_{v\in\mathbb{V}} (PC(p_{v,k}) + PC(c_{v,k})) \\
&\text{s.t.} \\
&0 \le Pch_{v,j,k} \le Pch^{\max}_{v,j,k},\ \forall\, v \in \mathbb{V},\ \forall\, j \in H, \text{ and } \forall\, k \\
&Pch_{j,k} = \sum_{v\in\mathbb{V}} Pch_{v,j,k} \le P^{j}_{\text{total}}, \forall\, k,\ \forall\, j \in H \\
&\sum_{j\in H} jPch_{j,k} \cdot r_j \le \Xi,\ \forall\, k \\
&0 \le P^{\text{init}}_{v,k} + \left(\sum_{j\in H} a \cdot Pch_{v,j,k} - PC(p_{v,k}) - PC(c_{v,k}) \right. \\
&\qquad \left. - P^{k}_{\text{cons}} \cdot \left(1 - \sum_{j\in H} x_{v,j,k} \right) \right) \\
&\quad \le C^{\max}_{\text{battery}},\ \forall\, v \in \mathbb{V},\ \forall\, k \\
&\frac{Pch_{v,j,k}}{Pch^{\max}_{v,j,k}} \le x_{v,j,k},\ \forall\, v \in \mathbb{V},\ \forall\, j \in H, \text{ and } \forall\, k \\
&\sum_{j\in H} x_{v,j,k} \le 1 \text{ and } x_{v,j,k} \in X = [0,1] \cap \mathbb{Z}, \\
&\qquad \forall\, v \in \mathbb{V},\ \forall\, j \in H, \text{ and } \forall\, k \\
&PC(p_{v,k}) + PC(c_{v,k}) \le P^{\text{init}}_{v,k},\ \forall\, v \in \mathbb{V}, \forall\, k \\
&\sum_k \sum_{j\in H} x_{v,j,k} \le X_{\max},\ \forall\, v \in \mathbb{V}
\end{aligned} \tag{24}$$

The constraints are according to (4)–(9), (14), and (23), respectively. And the transmission delay in VANETs is integrated in the constraint of (23).

V. The Coordinated Predictive EV Charging Strategy

In this section, we derive the solution of problem (24) to obtain the coordinated predictive EV charging strategy. The original problem (24) is a time-coupled mixed-integer linear programming (MILP) problem and thus very complicated to solve, however, having observed that the last constraint of (24) is the only time-coupled constraint, the original time-coupled MILP problem can be first time-decoupled into a series of sub-MILPs through Lagrange duality [25]. The optimal solutions of all the sub-MILPs can form a ϵ-optimal solution to the original problem [46]. In other words, with Lagrange duality, only solving the decoupled sub-MILP problem in each period can lead to an ϵ-optimal solution for the whole periods. Each sub-MILP can be further solved by the branch-and-cut-based outer approximation (BCBOA) algorithm [26]. The optimality of BCBOA is also proved.

A. Optimization Decoupling Based on Lagrange Duality

First, we decouple the original optimization problem (24) into a series of sub-problems with respect to period k by applying the Lagrange duality [25]. The basic idea is to add the time-coupled constraints of (24) into the objective function by augmenting the objective function with a weighted sum of the time-coupled constraint functions. In this way, the original problem can be time-decoupled into a series of sub-problems, each corresponding to a period k with only parameters and decision variables of that period. The intrinsic philosophy behind the ϵ-optimal solution to the original MILP after decoupling, is that the objective function is linear; and all the inequality constrains are linear [46]. We define the Lagrangian $L(.)$ associated with the problem (24) as

$$\begin{aligned}
L(Pch_{v,j,k}, x_{v,j,k}) = \sum_k \Bigg\{ &\sum_{v\in\mathbb{V}} \sum_{j\in H} a \cdot Pch_{v,j,k} \\
&- \sum_{v\in\mathbb{V}} (PC(p_{v,k}) + PC(c_{v,k})) \Bigg\} - \sum_{v\in\mathbb{V}} \iota_v \left[\sum_k \sum_{j\in H} x_{v,j,k} - X_{\max} \right]
\end{aligned} \tag{25}$$

where ι_v is the Lagrange multipliers associated with the vth inequality constraint

$$\sum_k \sum_{j\in H} x_{v,j,k} \le X_{\max}. \tag{26}$$

The vector set $\{\iota_v\}$ is called the dual variables or Lagrange multiplier vector. Rearranging (25), we can obtain

$$\begin{aligned}
&L(Pch_{v,j,k}, x_{v,j,k}) \\
&\quad = \sum_k \Bigg\{ \left(\sum_{v\in\mathbb{V}} \sum_{j\in H} a \cdot Pch_{v,j,k} \right) \\
&\qquad - \sum_{v\in\mathbb{V}} (PC(p_{v,k}) + PC(c_{v,k})) \\
&\qquad - \sum_{v\in\mathbb{V}} \iota_v \left[\sum_{j\in H} x_{v,j,k} \right] \Bigg\} + \sum_{v\in\mathbb{V}} \iota_v X_{\max}.
\end{aligned} \tag{27}$$

We further decouple the problem into a series of uncoupled sub-problems corresponding to each period k by means of dual decomposition [25], and let $D^k(\iota_v)$ denote the maximum value of Lagrangian $L(.)$ over $Pch_{v,j,k}$ and $x_{v,j,k}$ in period k, i.e.,

$$\begin{aligned}
D^k(\iota_v) = \max_{Pch_{v,j,k}, x_{v,j,k}} \Bigg\{ &\left(\sum_{v\in\mathbb{V}} \sum_{j\in H} a \cdot Pch_{v,j,k} \right) \\
&- \sum_{v\in\mathbb{V}} (PC(p_{v,k}) + PC(c_{v,k})) - \sum_{v\in\mathbb{V}} \iota_v \left[\sum_{j\in H} x_{v,j,k} \right] \Bigg\}.
\end{aligned} \tag{28}$$

Then, let Lagrangian dual function $D(\iota_v)$ be the maximum value of Lagrangian $L(.)$ over $Pch_{v,j,k}$ and $x_{v,j,k}$, then

$$D(\iota_v) = \sum_k D^k(\iota_v) + \sum_{v\in\mathbb{V}} \iota_v X_{\max}. \tag{29}$$

By minimizing the Lagrangian dual function over dual variable, ι_v, we can get the ϵ-optimal solution of (24).

$$\begin{aligned} \min_{\iota_v} \quad & D(\iota_v) \\ \text{s.t.} \quad & \iota_v \geq 0. \end{aligned} \tag{30}$$

As shown in [46], for a given ι_v, if the solution $Pch_{v,j,k}$ and $x_{v,j,k}$ is optimal in (28) and satisfies the time-coupled constraint of (26), the solution are the ϵ-optimal solution to the original problem, with $\epsilon = -\sum_{v\in\mathbb{V}} \iota_v[\sum_k \sum_{j\in H} x_{v,j,k} - X_{\max}]$.

B. Solving the Sub-MILP Problem Based on BCBOA Algorithm

From the observation of (28), the sub-optimization problem, P, see (31), shown at the bottom of the page, where x and Pch are the set of all $x_{v,j,k}$ and $Pch_{v,j,k}$, respectively.

Since the sub-optimization problem (31) is an MILP, it can be solved by the BCBOA Algorithm [26]. The BCBOA algorithm is an iterative procedure that solves the original MILP by solving an alternating sequence of relaxed MILPs and linear programs (LPs). The relaxed MILP is obtained from the original problem P by replacing the original constraints with linear functions by polyhedral outer approximations (OAs). The OA is to provide polyhedral representation of the feasible space of P. Such a representation will render linearly in the continuous variable, and enable to reduce the complexity of the original problem. Given any set of possible solutions $\mathbb{T} = \{(x^1, Pch^1), \ldots, (x^t, Pch^t), \ldots\}$, the MILP is given as follows,

$$P^{OA}(T) \begin{cases} \max \varpi \\ \text{s.t.} \\ \nabla G(x, Pch)^T_{|(x^t, Pch^t)} \begin{pmatrix} x - x^t \\ Pch - Pch^t \end{pmatrix} \\ \quad + G(x^t, Pch^t) \geq \varpi \\ \nabla F(x, Pch)^T_{|(x^t, Pch^t)} \begin{pmatrix} x - x^t \\ Pch - Pch^t \end{pmatrix} \\ \quad + F(x^t, Pch^t) \leq 0 \\ \forall (x^t, Pch^t) \in \mathbb{T},\ x \in X \cap Z^n, \\ 0 \leq Pch_{v,j,k} \leq Pch^{\max}_{v,j,k},\ \varpi \in R \end{cases} \tag{32}$$

$$P \begin{cases} \max\limits_{Pch_{v,j,k}, x_{v,j,k}} \left\{ \left(\sum\limits_{v\in\mathbb{V}} \sum\limits_{j\in H} a \cdot Pch_{v,j,k} \right) - \sum\limits_{v\in\mathbb{V}} (PC(p_{v,k}) + PC(c_{v,k})) - \sum\limits_{v\in\mathbb{V}} \iota_v \left[\sum\limits_{j\in H} x_{v,j,k} \right] \right\} \\ \text{s.t.} \\ f_{j,1}(x, Pch) = Pch_{j,k} = \sum\limits_{v\in\mathbb{V}} Pch_{v,j,k} - P^j_{\text{total}} \leq 0,\ \forall j \in H \\ f_2(x, Pch) = \sum\limits_{j\in H} Pch_{j,k} \cdot jr_j - \Xi \leq 0 \\ f_{v,3}(x, Pch) = P^{\text{init}}_{v,k} + \left(\sum\limits_{j\in H} a \cdot Pch_{v,j,k} - PC(p_{v,k}) - PC(c_{v,k}) - P^k_{\text{cons}} \left(1 - \sum\limits_j x_{v,j,k} \right) \right) - C^{\max}_{\text{battery}} \leq 0,\ \forall v \in \mathbb{V} \\ f_{v,4}(x, Pch) = -\left[P^{\text{init}}_{v,k} + \left(\sum\limits_{j\in H} a \cdot Pch_{v,j,k} - PC(p_{v,k}) - PC(c_{v,k}) - P^k_{\text{cons}} \left(1 - \sum\limits_j x_{v,j,k} \right) \right) \right] \leq 0,\ \forall v \in \mathbb{V} \\ f_{v,j,5}(x, Pch) = \frac{Pch_{v,j,k}}{Pch^{\max}_{v,j,k}} - x_{v,j,k} \leq 0,\ \forall v \in \mathbb{V},\ \forall j \in H \\ f_{v,6}(x, Pch) = \sum\limits_{j\in H} x_{v,j,k} - 1 \leq 0,\ \forall v \in \mathbb{V} \\ f_{v,7}(x, Pch) = PC(p_{v,k}) + PC(c_{v,k}) - P^{\text{init}}_{v,k} \leq 0,\ \forall v \in \mathbb{V} \\ 0 \leq Pch_{v,j,k} \leq Pch^{\max}_{v,j,k},\ x_{v,j,k} \in \{0, 1\},\ \forall v \in \mathbb{V},\ \forall j \in H \end{cases} \tag{31}$$

$$P_{\bar{x}} \begin{cases} \max G(\overline{x}, Pch) \\ \text{s.t.} \\ f_{j,1} = \sum\limits_{v\in\mathbb{V}} Pch_{v,j,k} - P^j_{\text{total}} \leq 0,\ \forall j \in H \\ f_2 = \sum\limits_{j\in H} (Pch_{j,k} \cdot jr_j) = \sum\limits_{j\in H} \left(\sum\limits_{v\in\mathbb{V}} Pch_{v,j,k} \cdot jr_j \right) - \Xi \leq 0 \\ f_{v,3} = P^{\text{init}}_{v,k} + \left(\sum\limits_{j\in H} a \cdot Pch_{v,j,k} - \overline{PC(p_{v,k})} - \overline{PC(c_{v,k})} - P^k_{\text{cons}} \left(1 - \sum\limits_j \overline{x_{v,j,k}} \right) \right) - C^{\max}_{\text{battery}} \leq 0,\ \forall v \in \mathbb{V} \\ f_{v,4} = -\left[P^{\text{init}}_{v,k} + \left(\sum\limits_{j\in H} a \cdot Pch_{v,j,k} - \overline{PC(p_{v,k})} - \overline{PC(c_{v,k})} - P^k_{\text{cons}} \left(1 - \sum\limits_j \overline{x_{v,j,k}} \right) \right) \right] \leq 0,\ \forall v \in \mathbb{V} \\ f_{v,j,5} = \frac{Pch_{v,j,k}}{Pch^{\max}_{v,j,k}} - \overline{x_{v,j,k}} \leq 0,\ \forall j \in H,\ \forall v \in \mathbb{V} \\ 0 \leq Pch_{v,j,k} \leq Pch^{\max}_{v,j,k} \end{cases} \tag{33}$$

where

$$G(x,Pch)=\left\{\left(\sum_{v\in\mathbb{V}}\sum_{j\in H}a\cdot Pch_{v,j,k}\right)-\sum_{v\in\mathbb{V}}\left(PC(p_{v,k})+PC(c_{v,k})\right)-\sum_{v\in\mathbb{V}}\iota_v\left[\sum_{j\in H}x_{v,j,k}\right]\right\},$$

$$F=\{f_{j,1},f_2,f_{v,3},f_{v,4},f_{v,j,5},f_{v,6},f_{v,7}\},\ \forall v\in\mathbb{V},\ \forall j\in H$$

and ϖ is an auxiliary variable. Here, $\nabla G(\cdot)^T$ denotes the transpose of the gradient of G.

The LP is obtained from the original problem P with x fixed to $\bar{x}$, where $\bar{x}$ is the optimal solution of x in MILP (32). In summary, the OA algorithm utilizes the gradients of the objective and constraint functions at different points to build a MILP relaxation of the problem. It should be noted that since all the functions in problem P were linear, the relaxed MILP at the first iteration would be identical to the original problem, and hence the BCBOA would terminate in at most two iterations. The following theorem shows that if 1) the solution set, $\mathbb{T}$, contains suitable points; 2) KKT conditions are satisfied at these points, the problems $P^{OA}(T)$ and P are equivalent.

Theorem 2: Consider that P has a finite set of optimal solutions. For all $\bar{x}\in X\cap Z^n$, if the problem, see (33), shown at the bottom of the previous page, is feasible, there exists $\overline{Pch}$ to be its optimal solution. Otherwise, if $P_{\bar{x}}$ is not feasible, $\overline{Pch}$ is as the optimal solution to the following problem

$$P^F_{\bar{x}}\begin{cases}\min \sum_{jj=1}^{|H|+1+2|\mathbb{V}|+|H||\mathbb{V}|} u_{jj}\\ \text{s.t. } f_{j,1}-u_{jj}\le 0,\ jj=\{1,\dots,|H|\},\ j\in H\\ f_2-u_{|H|+1}\le 0\\ f_{v,3}-u_{jj}\le 0,\ jj=\{|H|+2,\dots,|H|+1+|\mathbb{V}|\},\ v\in\mathbb{V}\\ f_{v,4}-u_{jj}\le 0,\\ \quad jj=\{|H|+2+|\mathbb{V}|,\dots,|H|+1+2|\mathbb{V}|\},\ v\in\mathbb{V}\\ f_{v,j,5}-u_{jj}\le 0,\ jj=\{|H|+2+2|\mathbb{V}|,\dots,\\ \quad |H|+1+2|V|+|\mathbb{V}||H|\},\ v\in\mathbb{V},\ j\in H\\ 0\le Pch_{v,j,k}\le Pch^{\max}_{v,j,k}\end{cases}\tag{34}$$

where each u_{jj} has one-to-one match with each linear constraint (i.e., $f_{j,1}$, f_2, $f_{v,3}$, $f_{v,4}$, and $f_{v,j,5}$) and there are totally $|H|+1+2|\mathbb{V}|+|H||\mathbb{V}|$ constraints except the constraint $0\le Pch_{v,j,k}\le Pch^{\max}_{v,j,k}$. Let $\bar{\mathbb{T}}$ be the set of all such solutions $(\bar{x},\overline{Pch})$. If the KKT conditions are satisfied at every point of $P_{\bar{x}}$, then P and $P^{OA}(\bar{\mathbb{T}})$ have the same optimal value.

Proof: Similar to [47], we denote X^F be the set of feasible $x\in X\cap Z^n$ in the problem $P_{\bar{x}}$ and X^I be the complement of X^F in $X\cap Z^n$. And $X^F\neq\emptyset$.

When $\bar{x}\in X^I$, the problem $P_{\bar{x}}$ is infeasible and therefore $\bar{\mathbb{T}}$ should contain the point $(\bar{x},\overline{Pch})$ with an optimal solution of $P^F_{\bar{x}}$. Therefore, $P^{OA}(\bar{\mathbb{T}})$ contains the constraint

$$\nabla F(x,Pch)^T_{|(\bar{x},\overline{Pch})}\begin{pmatrix}x-\bar{x}\\ Pch-\overline{Pch}\end{pmatrix}+F(\bar{x},\overline{Pch})\le 0$$
$$\text{where}\quad F=\{f_{j,1},f_2,f_{v,3},f_{v,4},f_{v,j,5},f_{v,6},f_{v,7}\},\quad\forall v\in\mathbb{V},\ \forall j\in H\tag{35}$$

In addition since $\overline{Pch}$ is an optimal solution of $P^F_{\bar{x}}$ and the KKT conditions are satisfied, there exists $\mu\in R_+^{2*[|H|+1+2|\mathbb{V}|+|H||\mathbb{V}||]}$ such that the first $|H|+1+2|\mathbb{V}|+|\mathbb{V}|\cdot|H|$ elements in μ has one-to-one match with each constraint in F and

$$\sum_{jj=1}^{|H|+1+2|\mathbb{V}|+|H||\mathbb{V}|}\mu_{jj}\nabla_{Pch}\left[f_{jj}(\bar{x},\overline{Pch})\right]=0,$$
$$\forall f_{jj}\in F=\{f_{j,1},f_2,f_{v,3},f_{v,4},f_{v,j,5}\},\ \forall v\in\mathbb{V},\ \forall j\in H.\tag{36}$$

$$1-\mu_{jj}-\mu_{|H|+1+2|\mathbb{V}|+|\mathbb{V}|\cdot|H|+jj}=0,\quad jj=1,\dots,|H|+1+2|\mathbb{V}|+|\mathbb{V}|\cdot|H|\tag{37}$$

$$\mu_{jj}\left[f_{jj}(\bar{x},\overline{Pch})-\bar{u}_{jj}\right]=0,\quad jj=1,\dots,|H|+1+2|\mathbb{V}|+|\mathbb{V}||H|\tag{38}$$

$$\mu_{|H|+1+2|\mathbb{V}|+|\mathbb{V}||H|+jj}\bar{u}_{jj}=0,\quad jj=1,\dots,|H|+1+2|\mathbb{V}|+|\mathbb{V}||H|.\tag{39}$$

Based on (35), we further have

$$\nabla_{Pch}\left[f_{jj}(\bar{x},\overline{Pch})\right]^T(Pch-\overline{Pch})+f_{jj}(\bar{x},\overline{Pch})\le 0,\quad jj=1,\dots,|H|+1+2|\mathbb{V}|+|H||\mathbb{V}|,\ \forall f_{jj}\in F.\tag{40}$$

Adding $|H|+1+2|\mathbb{V}|+|H||\mathbb{V}|$ inequalities in (40) with the nonnegative multipliers $\mu_1,\dots,\mu_{|H|+1+2|\mathbb{V}|+|H|\cdot|\mathbb{V}|}$, after rearranging, we obtain

$$\sum_{j=1}^{|H|+1+2|\mathbb{V}|+|H||\mathbb{V}|}\mu_{jj}\nabla_{Pch}\left[f_{jj}(\bar{x},\overline{Pch})\right]^T(Pch-\overline{Pch})\le-\sum_{j=1}^{|H|+1+2|\mathbb{V}|+|H||\mathbb{V}|}\mu_{jj}f_{jj}(\bar{x},\overline{Pch}),\ \forall f_{jj}\in F.\tag{41}$$

Based on (36), the left hand side of (41) equals to zero. While based on (38), the right hand side of (41) equals to $-\sum_{jj=1}^{|H|+1+2|\mathbb{V}|+|H||\mathbb{V}|}\mu_{jj}\bar{u}_{jj}$. From (39), $\mu_{jj+|H|+1+2|\mathbb{V}|+|\mathbb{V}||H|}=0$ if $\overline{u_{jj}}>0$, $\forall jj\in\{1,\dots,|H|+1+2|\mathbb{V}|+|\mathbb{V}||H|\}$. Then, combining (37), we get $\mu_{jj}=1$ for $\forall jj\in\{1,\dots,|H|+1+2|\mathbb{V}|+|\mathbb{V}||H|\}$ that satisfies $\overline{u_{jj}}>0$. This implies that the RHS of (41), i.e., $-\sum_{jj=1}^{|H|+1+2|\mathbb{V}|+|\mathbb{V}||H|}\bar{u}_{jj}$, is strictly negative otherwise $P_{\bar{x}}$ would be feasible. Therefore, the inequality (41) has no solution. This implies that the maximum value of $P^{OA}(\bar{\mathbb{T}})$ is to be found as the maximum value over all $x\in X^F$.

Furthermore, let $\overline{Pch}$ be an optimal solution to $P_{\bar{x}}$. $(G(\bar{x},\overline{Pch}),\bar{x},\overline{Pch})$ is a feasible solution of $P^{OA}_{\bar{x}}(\bar{\mathbb{T}})$. Therefore,

(a)

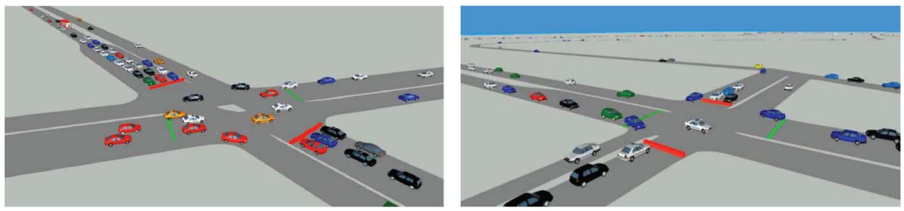

(b)

Fig. 4. The simulation scenario of University of Waterloo region in VISSIM. (a) A snap shot of the simulation region with signing the simulated roads in blue. (b) The 3D vehicle traffic illustrations of two intersections highlighted in red on the upside.

TABLE I
AN EXAMPLE OF ACTIVE AND REACTIVE POWER VALUE AT EACH BUS OF THE SYSTEM

Hour	Bus Number	2	3	4	5	6	7	8	9	10	11	12
21:00	P(MW)	TBD	4.0	5.5	-	6.0	5.5	4.5	-	3.5	TBD	3.0
	Q(MVar)	-	3.0	5.5	-	1.5	5.5	4.5	-	3.0	-	1.5

$G(\bar{x}, \overline{Pch})$ is a lower bound on the optimal value ϖ of $P_{\bar{x}}^{OA}(\bar{\mathbb{T}})$. Next this value $G(\bar{x}, \overline{Pch})$ will be proved to be also an upper bound, i.e., $\varpi \leq G(\bar{x}, \overline{Pch})$. When $\overline{Pch}$ is an optimal solution of $P_{\bar{x}}$ and satisfies the KKT conditions. There exists $\mu \in \mathbb{R}_{+}^{|H|+1+2|\mathbb{V}|+|\mathbb{V}||H|}$ such that

$$-\nabla_{Pch} G(\bar{x}, \overline{Pch}) + \sum_{jj=1}^{|H|+1+2|\mathbb{V}|+|\mathbb{V}||H|} \mu_{jj} \nabla_{Pch} \left[f_{jj}(\bar{x}, \overline{Pch}) \right] = 0, \ \forall f_{jj} \in F \tag{42}$$

$$\mu_{jj} f_{jj}(\bar{x}, \overline{Pch}) = 0, \ jj = 1, \ldots, |H| + 1 + 2|\mathbb{V}| + |\mathbb{V}||H|. \tag{43}$$

By outer-approximation programming, any solution of $P_{\bar{x}}^{OA}(\bar{\mathbb{T}})$ should satisfy

$$\begin{aligned} &-\nabla_{Pch} G(\bar{x}, \overline{Pch})^T (Pch - \overline{Pch}) - G(\bar{x}, \overline{Pch}) \leq -\varpi \\ &\nabla_{Pch} \left[f_{jj}(\bar{x}, \overline{Pch}) \right]^T (Pch - \overline{Pch}) + f_{jj}(\bar{x}, \overline{Pch}) \leq 0, \\ &\quad jj = 1, \ldots, |H| + 1 + 2|\mathbb{V}| + |\mathbb{V}||H| \end{aligned} \tag{44}$$

Multiplying the second inequality set in (44) by the Lagrange multipliers (i.e., $\mu_{jj} \geq 0$) and then adding to the first inequality in (44), we rearrange the left hand side and obtain

$$\left\{ -\nabla_{Pch} G(\bar{x}, \overline{Pch}) + \sum_{j=1}^{|H|+1+2|\mathbb{V}|+|\mathbb{V}||H|} \mu_{jj} \nabla_{Pch} f_{jj}(\bar{x}, \overline{Pch}) \right\}^T \cdot (Pch - \overline{Pch}) + \sum_{j=1}^{|H|+1+2|\mathbb{V}|+|\mathbb{V}||H|} \mu_{jj} f_{jj}(\bar{x}, \overline{Pch}) - G(\bar{x}, \overline{Pch})$$

$$= -G(\bar{x}, \overline{Pch}) \leq -\varpi. \tag{45}$$

From (42) and (43), the left hand side of (45) is equivalent to $-G(\bar{x}, \overline{Pch})$. Therefore, we get $G(\bar{x}, \overline{Pch}) \geq \varpi$. In other words, for any $\bar{x} \in X^F$, the problem $P_{\bar{x}}^{OA}(\bar{\mathbb{T}})$ and $P_{\bar{x}}$ have the same objective value. ■

Therefore, the optimality of BCBOA is proved. In summary, the proposed charging strategy can be obtained by first time-decoupling the original problem into a series of sub-MILPs through Lagrange duality, and then solving the sub-MILPs based on the branch-and-cut-based outer approximation (BCBOA) algorithm. The charging decisions in terms of $Pch_{v,j,k}$ and $x_{v,j,k}$ are dispatched to each EV via VANETs.

VI. PERFORMANCE EVALUATION

We consider a realistic suburban scenario as shown in Fig. 4, which is the region around the campus of University of Waterloo (Waterloo, ON, Canada). RSUs are uniformly deployed along roads, and two charging stations are deployed as marked in Fig. 4(a). The parameters of the 12-bus distribution system (only load buses) in [35] are considered, with the load enlarged to MW level. Two charging stations are connected to Bus_2 and Bus_{11}, respectively. Loads connected at each bus at 21:00 is given in Table I. The input voltage is set to 1.0 pu, and the minimum allowable voltage is 0.9 pu, with

TABLE II
NORMALIZED POWER OVER THE POWER AT 21:00 FOR ALL THE BUSES WITHOUT EV CHARGING LOAD DURING A DAY

Hour	1:00	2:00	3:00	4:00	5:00	6:00	7:00	8:00	9:00	10:00	11:00	12:00
Normalized Power	0.5	0.5	0.5	0.5	0.7	0.9	1.3	1.5	2.1	2.3	2.5	2.5
Hour	13:00	14:00	15:00	16:00	17:00	18:00	19:00	20:00	21:00	22:00	23:00	24:00
Normalized Power	2.5	2.3	2.1	1.8	1.5	1.4	1.3	1.2	1.0	0.7	0.7	0.7

the impedance of any line section being $0.005 + j0.0046$. The normalized power over the power at 21:00 for all the buses without EV charging load is shown in Table II, according to the trend in [48]. Vehicles move in this region following the aforementioned mobility model in Section III-C. To model the vehicle traffic, a highly-realistic microscopic vehicle traffic simulator, VISSIM [27], is employed to generate vehicle trace files for recording the vehicle mobility characteristics. Based on the trace files, we first evaluate the average transmission delay incurred by VANETs for an EV to receive a charging decision. Then, combining the power system data, we investigate the performance of our proposed EV charging strategy, using a custom simulator built in Matlab. The proposed strategy is compared to an existing coordinated charging strategy without considering the EV mobility and the travel cost [15]. The compared performance metrics include the total EV charging energy (TECE), the average EV travel cost (AETC), and the percentage of EVs that succeed or fail in charging.

A. Simulation Setup

To simulate a VANET with VISSIM, vehicles are pushed into the region of 6000 m $*$ 2800 m, as shown in Fig. 4(a). At the beginning of the simulation, vehicles enter the region from the preseted entries (e.g., 9 entries at the ends of main roads), following a Poisson process at a rate ζ (e.g., $\zeta = 2500$ vehicle/hour/entry). After a certain duration t_ζ (e.g., 240 s), the vehicle pushing-in stops to reach the density 30 vehicle/km/lane. The information (e.g., locations, velocities, etc.) of vehicles can be recorded at the end of every simulation step (e.g., 0.2 s) in the recorded trace files. In addition, a set of RSUs (e.g., 25 RSUs) is deployed uniformly along roads in the region, with the transmission range of R (e.g., 150 m). And the total simulation time is 3000 s.

The car following model, Wiedemann 74 model [49], is utilized for modeling the traffic; the vehicle acceleration is a function of the vehicle velocity, the characteristics of the driver (or the vehicle), and the difference in distance and velocity between the subject vehicle and the vehicle in front [49]. At an intersection, the vehicle traffic is controlled either by a traffic light or a stop sign based on the reality, as shown in Fig. 4(b). The velocity distribution for all vehicles follows the velocity model described in Section III-C with parameters $V = \{v_L, v_H\}$ and D (e.g., taking $v_L = 30$ km/hour, $v_H = 60$ km/hour, $D = 60$ s as a case study).

Besides, in the EV charging simulations, we set the EV battery capacity to 85 KWh according to the TESLA Model S [3]. The charging period is set as 30 min as a case study, with the maximum charging energy of 30 KWh. If an EV is not scheduled for charging in a period, the energy cost for running on the road in that period is set to be uniformly distributed within [0,10] KWh. And the maximal charging times for EVs i.e., $X_{\max}$, is set as 3. To better illustrate the performance of the proposed charging strategy, the centralized charging strategy in [15] is compared where the optimization objective is to only maximize the total amount of EV charging energy.

B. Simulation Results of VANETs

Based on the trace files obtained from VISSIM, Fig. 5(a) shows the probability density function (PDF) of vehicle headway distance under the above simulation settings when $\zeta = 2500$ vehicles/hour/entry. It is shown that the PDF of the headway distance matches well with an exponential distribution, which validates the premise in Section III-C that the headway distance follows an exponential distribution when the vehicle density is low or medium. Besides, from the exponential distribution in Fig. 5(a), the average headway distance is about 30 m, which is very close to that calculated from the predefined vehicle density in the simulation setting, i.e., 30 vehicles/km/lane. In addition, the theoretical PDF of the distance from the last hop vehicle to the nearest RSU for one delivery (through (18)) is further verified by Fig. 5(b). With 25 RSUs deployed in the network, the theoretical PDF is calculated with the parameters in the simulation setting based on (18). The simulated PDF is obtained from the real trace files of VISSIM. In Fig. 5(b), it can be seen that the simulated PDF matches well with the theoretical one, which validates the effectiveness of the theoretical analysis in (18). Also, according to the simulation, the average distance from the last hop vehicle to its neatest RSU is around 200 m.

When the vehicle density is reduced, e.g., $\zeta = 1800$ vehicle/hour/entry, the PDF of the headway distance is shown in Fig. 5(c), approximately following an exponential distribution as well. And the average distance is increased to 46 m. Furthermore, the PDF of the last-hop V2R distance is illustrated in Fig. 5(d), and the average V2R distance of the last hop is about 215 m. The average V2R distance also matches with the analytical results in (18). Therefore, Fig. 5 validates the mobility model proposed in Section III-C as well as the analytical results of (18) which is derived based on the the proposed mobility model.

We then investigate the single-hop connection probability between a vehicle and its nearest RSU and the end-to-end multi-hop transmission delay in VANETs. The results are shown in Figs. 6 and 7, respectively, under different RSU deployments (i.e., 25 or 8 RSUs are deployed in the network) and different vehicle densities (i.e., $\zeta = 2500$ vehicles/hour/entry or $\zeta = 1800$). It can be observed from Fig. 6 that for a given number of RSUs and ζ, the connection probability increases with larger RSU transmission range. Besides, if the RSU transmission range is fixed, larger number of RSUs and larger ζ

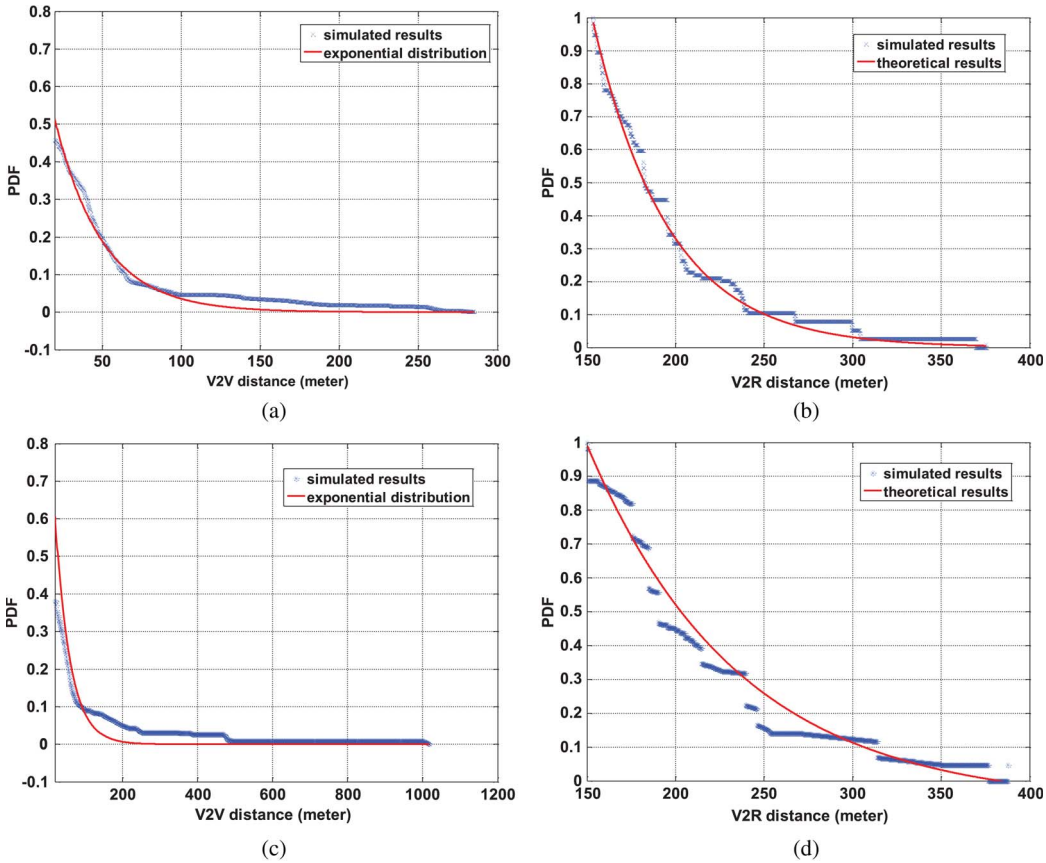

Fig. 5. The PDFs of both two adjacent vehicle distance (V2V distance) and the last hop V2R distance. (a) The PDF of V2V distance when $\zeta = 2500$. (b) The PDF of the last hop V2R distance when $\zeta = 2500$. (c) The PDF of V2V distance when $\zeta = 1800$. (d) The PDF of the last hop V2R distance when $\zeta = 1800$.

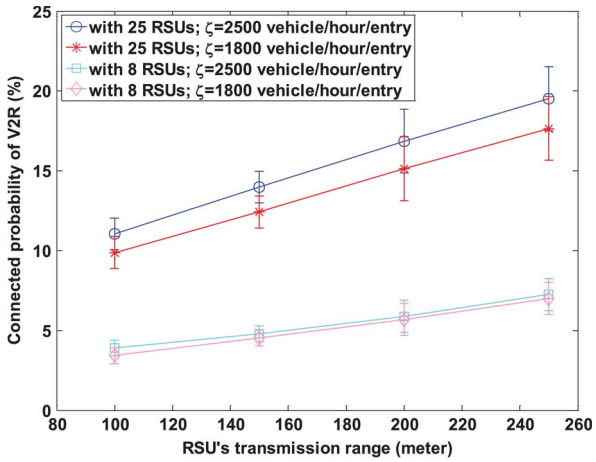

Fig. 6. The average connected probability between a vehicle and an RSU.

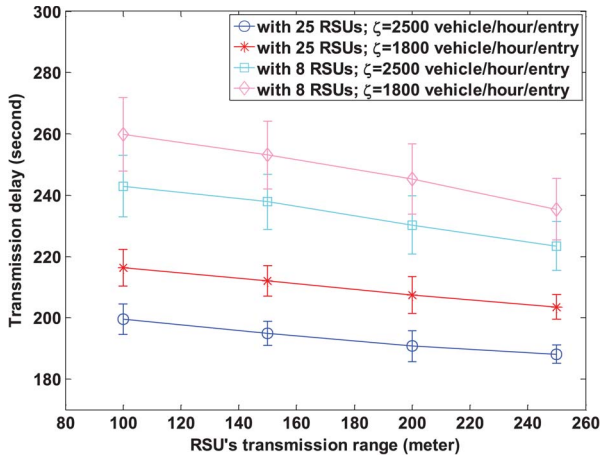

Fig. 7. The average transmission delay for a V2R uplink.

will both increase the single-hop connected probability but to different extents, i.e., the variation of the number of RSUs has larger impact on the connected probability than that of ζ. This can be explained as follows. As the collisions can be avoided according to the transmission model in Section III-D, the increase of ζ will affect the connected probability only through decreasing the average U_{off} as given in (18). Since the average headway distances under $\zeta = 2500$ and $\zeta = 1800$ are around 30 and 50, respectively, which are relatively small compared to the RSU transmission range, the two headway distances can be viewed as in the same scaling order. As a result, the average U_{off} will not change much under the two ζ values, leading to very small gaps in the connected probabilities when the number of RSUs is fixed. On the contrary, when ζ is fixed, different numbers of RSUs will result in big difference in the average U_{off}, leading to a much larger gap.

On the other hand, it can be seen in Fig. 7 that the average end-to-end transmission delay decreases when the RSU transmission range, the number of RSUs or ζ increases. More interestingly, different from the single-hop connected probabilities, the transmission delay does not increase much even when the number of RSUs is largely reduced, e.g., from 25 to 8.

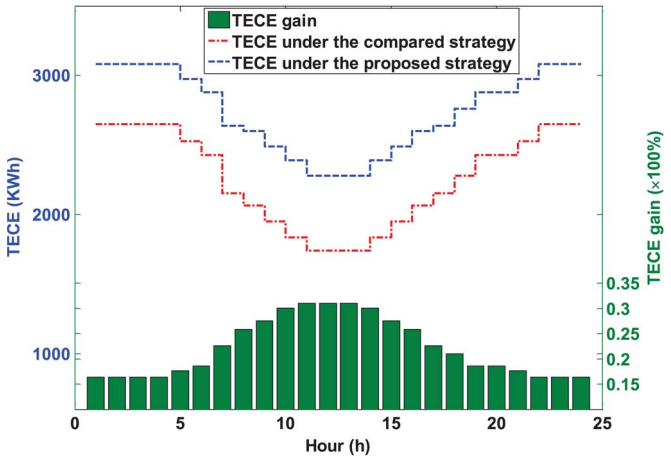

Fig. 8. Daily TECE comparison when the total number of EVs is fixed to 1200.

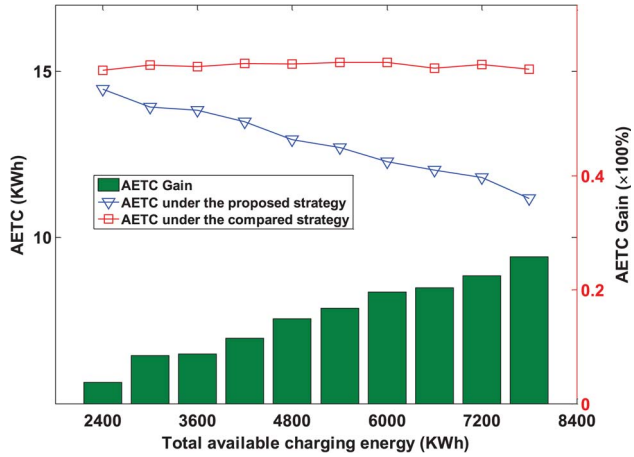

Fig. 9. AETC comparison with increasing TACE when the total number of EVs is 1200.

For example, the transmission delay is around 190 s with 25 RSUs and $\zeta = 2500$, and is around 240 s with 8 RSUs and $\zeta = 1800$. The small change compared to the big gap of connected probability is due to the benefits of multi-hop V2V relaying. When the number of RSU largely decreases, although the single-hop connection opportunities from a vehicle to the RSU is largely reduced, the information can still be efficiently delivered to the RSU through multi-hop V2V relaying at the cost of small delay increase. In other words, the multi-hop V2V relaying increases the equivalent transmission range of a vehicle. Besides, for the considered settings, the average transmission delay is around 200 s. Thus, although the transmission delay of VANETs is larger than the cellular systems, it is still tolerable for the applications of vehicle information collection compared to the decision making period (i.e., 30 min). More importantly, VANETs can considerably cut down the service cost and enhance the transmission rates, which is more important for the large-volume vehicle data collection.

C. Simulation Results of the Proposed Charging Strategy

In this subsection, we investigate the performance of the proposed charging strategy. As a case study, the strategy is conducted every 30 mins, and the simulation results are collected every one hour. This conducted period can be set differently for different requirements, with corresponding communication infrastructure deployment. We first study the TECE performance under a weekday total-available-charging-energy (TACE) profile [48] (see Table II) with fixed total number of EVs, as shown in Fig. 8. As we mainly focus on the behaviors of charging strategies when the overload is likely to occur, we only consider the case where the TACE is not enough to charge all the EVs in each period. It can be observed from Fig. 8 that for all the hours the proposed strategy can obtain larger TECE than the compared strategy. Since the compared strategy has no real-time vehicle information, the charging decision is made without considering the EV mobility and the travel cost. As a result, some EVs may be dispatched to a charging station that is too far to reach based on their current battery levels, making EV batteries depleted on the way and fail to be charged. On the contrary, our strategy considers the travel cost based on the vehicle information from VANETs and dispatches the EVs only to the charging stations within their reach, thus having a larger TECE. Besides, TECE gain is from 15% to 30% for different TACE, and is larger with smaller TACE. The reason is as follows. When the TACE is smaller, the number of EVs that cannot be charged in the current period is larger. As the EVs are mobile, they will continue to consume battery energy even if they are not charged. As a result, the average initial battery level is lower in the next period, and the depletion probability if an EV is dispatched to a farther station is larger under the compared strategy. As our strategy always avoids the EV depletion situation, the gain will be larger when the TACE is smaller.

Besides, we compare the AETC under different TACE in Fig. 9. It can be seen that the AETC of the proposed strategy is smaller than that of the compared strategy, and the gain is larger with larger TACE. As the proposed strategy considers to reduce the AETC and thus gives preference to closer charging stations, the AETC is lower than that under the compared strategy without considering the travel cost. When the TACE is increased, each charging station can accommodate more EVs. As a result, more EVs can be dispatched to the closer charging stations under the proposed strategy, resulting in a lower AETC (i.e., a larger gain) over the compared strategy.

We further compare the number of EVs that succeed and fail in charging under different strategies, respectively, as shown in Fig. 10. It can be observed that compared with the existing strategy, the proposed strategy achieves a smaller total number of involved EVs (i.e., the number of successfully charged EVs plus the number of EVs that fail to be charged) but a larger number of successfully charged EVs. This observation further corroborates the explanation for Fig. 8. Under the proposed strategy, as the EVs tend to be assigned to the closer stations, the load assignment is less balanced than the compared strategy. Thus the total number of involved EVs is smaller under the proposed strategy. However, as some involved EVs' batteries may be depleted on the way under the compared strategy, the EVs that actually succeed in charging are more in the proposed strategy. Therefore, it is essential to incorporate EV mobility into the optimal charging strategy design.

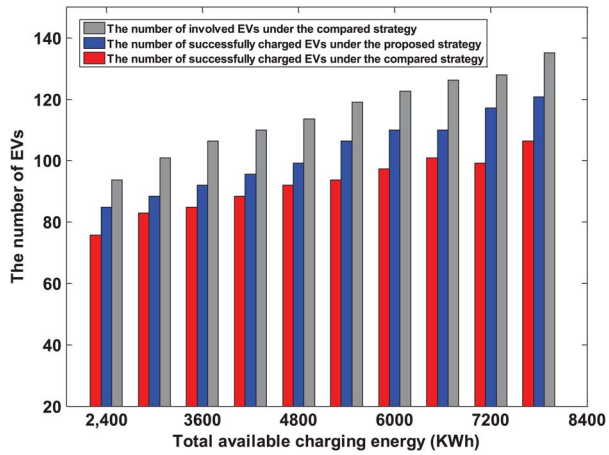

Fig. 10. Comparison of the number of involved EVs and successfully charged EVs, with 1200 EVs.

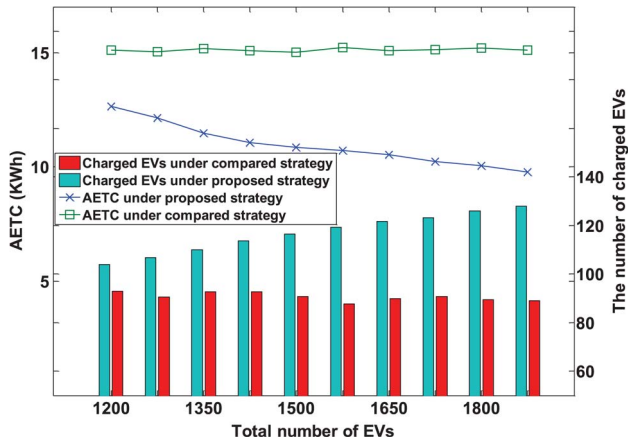

Fig. 11. Comparison of AETC and the number of successfully charged EVs, with fixed TACE (5400 KWh).

Last, with fixed TACE and increasing total number of EVs, we show the comparison of the AETC performance as well as the number of successfully charged EVs in Fig. 11. It can be observed that when TACE is fixed and the total number of EVs increases, the AETC of the proposed strategy decreases, and the number of successfully charged EVs increases; while both the two items remain almost unchanged under the compared strategy. As the proposed strategy considers to reduce the AETC, when the total number of EVs increases, more EVs that are closer to the charging stations are selected for charging. Thus, the AETC will decrease correspondingly. As the AETC decreases, the average battery level when the dispatched EVs arrive at the charging stations is higher, resulting in a smaller average EV charging energy. Thus more EVs can be dispatched and charged when the TACE is fixed. For the compared strategy, as it does not consider the AETC, increasing the total number of EVs has no impact on the EV selection, thus the performance remains almost unchanged.

VII. Conclusion

In this paper, we have incorporated the EV mobility into the EV charging and developed a VANET-enhanced coordinated EV charging strategy to improve the energy utilization and reduce the EV travel cost while averting the power system overloading. In specific, we first introduced a VANET-enhanced smart grid with the functionalities of real-time vehicle information collection through VANETs. Then, a predictive mobility-aware coordinated EV charging strategy was proposed to maximize the overall charging-energy-minus-travel-cost with power system overloading avoidance. Extensive simulations have been conducted to evaluate the cost incurred by the transmission delay in VANETs and demonstrate that the proposed EV charging strategy can achieve better performance than the existing strategy without considering the EV mobility and travel cost in terms of the total EV charging power, average EV travel cost and the number of successfully charged EVs. In our future work, we intend to study the incentive mechanisms for stimulating the EVs to follow the charging decisions to achieve the global optimality.

Acknowledgment

This research work is financially supported by Natural Sciences and Engineering Research Council of Canada (NSERC), Collaborative Research and Development (CRD) Grants, Canada.

References

[1] M. Wang, H. Liang, R. Deng, R. Zhang, and X. Shen, "VANET based online charging strategy for electric vehicles," in *Proc. IEEE GLOBECOM*, Atlanta, GA, USA, Dec. 2013, pp. 5115–5120.

[2] I. S. Bayram, G. Michailidis, M. Devetsikiotis, and F. Granelli, "Electric power allocation in a network of fast charging stations," *IEEE J. Sel. Areas Commun., Smart Grid Commun. Series*, vol. 31, no. 7, pp. 1235–1246, Jul. 2013.

[3] TESLA Motors. [Online]. Available: http://www.teslamotors.com/Pages/goelectric#

[4] Hybrid Cars, A Comprehensive Guide to Plug-in Hybrid Vehicles, 2011. [Online]. Available: http://www.hybridcars.com/plug-in-hybrid-cars/#battery

[5] Electric Power Resech Institute. [Online].Available: http://www.epri.com/Pages/Default.aspx

[6] A. Heider and H. J. Haubrich, "Impact of wide-scale EV charging on the power suppy network," in *Proc. IEE Colloqium Elect. Veh.-Technol. Roadmap Future*, 1998, vol. 6, pp. 1–4.

[7] K. Nyns, E. Haesen, and J. Driesen, "The impact of charging plug-in hybrid electric vehicles on a residential distribution grid," *IEEE Trans. Power Syst.*, vol. 25, no. 1, pp. 371–380, Feb. 2010.

[8] H. Liang, B. J. Choi, W. Zhuang, and X. Shen, "Optimizing the energy delivery via V2G systems based on stochastic inventory theory," *IEEE Trans. Smart Grid*, vol. 4, no. 4, pp. 2230–2243, Dec. 2013.

[9] P. Richardson, D. Flynn, and A. Keane, "Optimal charging of electric vehicles in low voltage distribution systems," *IEEE Trans. Power Syst.*, vol. 27, no. 1, pp. 268–279, Feb. 2012.

[10] J. Lopes, S. Polenz, C. Moreira, and R. Cherkaoui, "Identification of control and management strategies for LV unbalanced microgrids with plugged-in electric vehicles," *Elect. Power Syst. Res.*, vol. 80, no. 8, pp. 898–906, Feb. 2010.

[11] M. Shaaban, Y. Atwa, and E. El-Saadany, "PEVs modeling and impacts mitigation in distribution networks," *IEEE Trans. Power Syst.*, vol. 28, no. 2, pp. 1122–1131, May 2013.

[12] D. Ban, G. Michailidis, and M. Devetsikiotis, "Demand response control for PHEV charging stations by dynamic price adjustments," in *Proc. IEEE Innov. Smart Grid Technol.*, Washington, DC, USA, Jan. 2012, pp. 1–8.

[13] R. C. Green, L. Wang, and M. Alam, "The impact of plug-in hybrid electric vehicles on distribution networks: A review and outlook," *J. Renew. Sustain. Energy Rev.*, vol. 15, no. 1, pp. 544–553, Jan. 2011.

[14] G. T. Heydt, "The impact of electric vehicle deployment on load management strategies," *IEEE Trans. Power App. Syst.*, vol. PAS-102, no. 5, pp. 1253–1259, May 1983.

[15] P. Richardson, D. Flynn, and A. Keane, "Local versus centralized charging strategies for electric vehicles in low voltage distribution systems," *IEEE Trans. Smart Grid*, vol. 3, no. 2, pp. 1020–1028, Jun. 2012.
[16] K. Mets, T. Verschueren, W. Haerick, C. Develder, and F. Turck, "Optimizing smart energy control strategies for plug-in hybrid electric vehicle charging," in *Proc. IEEE Netw. Oper. Manag. Symp. Workshops*, Osaka, Japan, Apr. 2010, pp. 293–299.
[17] K. Clement, E. Haesen, and J. Driesen, "Coordinated charging of multiple plug-in hybrid electric vehicles in residential distribution grids," in *Proc. IEEE Power Syst. Conf. Expo.*, Seattle, WA, USA, Mar. 2009, pp. 1–7.
[18] L. Kelly, "Probabilistic modeling of plug-in hybrid electric vehicle impacts on distribution networks in British Columbia," M.S. thesis, Dept. Mech. Eng., Univ. Victoria, Victoria, BC, Canada, 2009.
[19] S. Bae and A. Kwasinski, "Spatial and temporal model of electric vehicle charging demand," *IEEE Trans. Smart Grid*, vol. 3, no. 1, pp. 394–403, Mar. 2012.
[20] H. Liang and W. Zhuang, "Efficient on-demand data service delivery to high-speed trains in cellular/infostation integrated networks," *IEEE J. Sel. Areas Commun.*, vol. 30, no. 4, pp. 780–791, May 2012.
[21] T. H. Luan, X. Shen, and F. Bai, "Integrity-oriented content transmission in the vehicular Ad Hoc networks," in *Proc. IEEE INFOCOM*, Turin, Italy, Apr. 2013, pp. 2562–2570.
[22] H. Liang and W. Zhuang, "Double-loop receiver-initiated MAC for cooperative data dissemination via roadside WLANs," *IEEE Trans. Commun.*, vol. 60, no. 9, pp. 2644–2656, Sep. 2012.
[23] H. T. Cheng, H. Shan, and W. Zhuang, "Infotainment and road safety service support in vehicular networking: From a communication perspective," *Mech. Syst. Signal Process., Special Issue Integr. Veh. Dyn.*, vol. 25, no. 6, pp. 2020–2038, Aug. 2011.
[24] T. H. Luan, X. Ling, and X. Shen, "Provisioning QoS controlled media access in vehicular to infrastructure communications," *Ad Hoc Netw.*, vol. 10, no. 2, pp. 231–242, Mar. 2012.
[25] S. Boyd and L. Vandenberghe, *Convex Optimization*. Cambridge, U.K.: Cambridge Univ. Press, 2004.
[26] M. Duran and I. Grossmann, "An outer-approximation algorithm for a class of mixed-integer nonlinear programs," *Math. Programm.*, vol. 36, no. 3, pp. 307–339, Dec. 1986.
[27] [Online]. Available: http://vision-traffic.ptvgroup.com/en-uk/products/ptv-vissim/
[28] J. Herrera, D. Work, R. Herring, X. Ban, and A. Bayen, "Evaluation of traffic data obtained via GPS-enabled mobile phones: The mobiltiy century field experiment," Univ. California, Berkeley Inst. Transp. Studies, Berkeley, CA, USA, Working Paper UCB-ITS-VWP-2009-8, Aug. 2009.
[29] R. Herring, A. Hofleitner, and S. Amin, "Using mobile phones to forecast arterial traffic through statistical learning," in *Proc. 89th Annu. Meet. Transp. Res. Board*, Washington, DC, USA, no. 10-2493, Jan. 2010.
[30] K. Lee, J. Lee, Y. Yi, I. Rhee, and S. Chong, "Mobile data offloading: How much can wifi deliver?" in *Proc. ACM Co-NEXT*, Nov. 2010, pp. 425–426.
[31] H. Liu, A. Danczyk, R. Brewer, and R. Starr, "Evaluation of cell phone traffic data in Minnesota," *Transp. Res. Rec.*, vol. 2086, no. 1, pp. 1–7, Dec. 2008.
[32] N. Lu *et al.*, "Vehicles meet infrastructure: Toward capacity-cost tradeoffs for vehicular access networks," *IEEE Trans. Intell. Transp. Syst.*, vol. 14, no. 3, pp. 1266–1277, Sep. 2013.
[33] M. Wang *et al.*, "Throughput capacity of VANETs by exploiting mobility diversity," in *Proc. IEEE ICC*, Ottawa, ON, Canada, Jun. 2012, pp. 4980–4984.
[34] N. Lu, T. Luan, M. Wang, X. Shen, and F. Bai, "Bounds of asymptotic performance limits of social-proximity vehicular networks," *IEEE/ACM Trans. Netw.*, vol. 22, no. 3, pp. 812–825, Jun. 2011.
[35] M. E. Elkhatb, R. El-Shatshat, and M. Salama, "Novel coordinated voltage control for smart distribution network with DG," *IEEE Trans. Smart Grid*, vol. 2, no. 4, pp. 598–605, Dec. 2011.
[36] L. Cheng, B. E. Henty, D. D. Stancil, F. Bai, and P. Mudalige, "Mobile vehicle-to-vehicle narrow-band channel measurement and characterization of the 5.9 GHz dedicated short range communication (DSRC) frequency band," *IEEE J. Sel. Areas Commun.*, vol. 25, no. 8, pp. 1501–1516, Oct. 2007.
[37] A. Abdrabou and W. Zhuang, "Probabilistic delay control and road side unit placement for vehicular Ad Hoc netowrks with disrupted connectivity," *IEEE J. Sel. Areas Commun.*, vol. 29, no. 1, pp. 129–139, Jan. 2011.
[38] A. May, *Traffic Flow Fundamentals*. Englewood Cliffs, NJ, USA: Prentice-Hall, 1990.
[39] N. Wisitpongphan, F. Bai, P. Mudalige, V. Sadekar, and O. Tonguz, "Routing in sparse vehicular Ad Hoc networks," *IEEE J. Sel. Areas Commun.*, vol. 25, no. 8, pp. 1538–1556, Oct. 2007.
[40] O. Hafez, "Some Aspects of Microgrid Planning and Optimal Distribution Operation in the Presence of Electric Vehicles," M.S. thesis, Dept. Electrical and Computer Eng., Univ. Waterloo, Waterloo, ON, Canada, 2011.
[41] R. Nelson, "Power requirements for batteries in hybrid electric vehicles," *IEEE J. Power Source*, vol. 91, no. 1, pp. 2–26, Nov. 2000.
[42] *Draft Amendement to Part 11: Wireless Medium Access Control (MAC) and Physical Layer (PHY) specifications: Wireless Access in Vehicular Environments*, IEEE 802.11p/D2.01, Mar. 2007, IEEE WG.
[43] R. Deng, Z. Yang, J. Chen, and M. Chow, "Load scheduling with price uncertainty and temporally-coupled constraints in smart grids," *IEEE Trans. Power Syst.*, no. 99, Mar. 2014.
[44] R. Deng, Z. Yang, J. Chen, N. Asr, and M. Chow, "Residential energy consumption scheduling: A coupled-constraint game approach," *IEEE Trans. Smart Grid*, vol. 5, no. 3, pp. 1340–1350, May 2014.
[45] M. Abboud, L. Jaoude, and Z. Kerbage, "Real time GPS navigation system," in *Proc. 3rd FEA Student Conf.*, 2004, pp. 1–6.
[46] A. Geoffrion, "Lagrangean relaxation for integer programming," *Math. Programm. Study*, vol. 2, pp. 82–114, 1974.
[47] P. Bonami *et al.*, "An algorithmic framework for convex mixed integer nonlinear programs," *J. Discr. Optim.*, vol. 5, no. 2, pp. 186–204, May 2008.
[48] C. Norén and J. Pyrko, "Typical load shapes for Swedish schools and hotels," *Energy Buildings*, vol. 28, no. 2, pp. 145–157, Oct. 1998.
[49] R. Wiedemann, "Modeling of RTI-elements on multi-lane roads," in *Proc. Drive Conf.*, Brussels, Belgium, Feb. 1991, pp. 1001–1011.

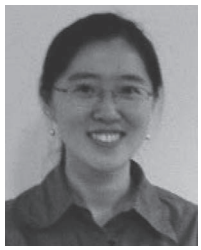

Miao Wang received the B.Sc. degree from Beijing University of Posts and Telecommunications, Beijing, China, and the M.Sc. degree from Beihang University, Beijing, in 2007 and 2010, respectively. She is currently working toward the Ph.D. degree with the Department of Electrical and Computer Engineering, University of Waterloo, Waterloo, ON, Canada. Her current research interests include the capacity and delay analysis in vehicular networks and electrical vehicle charging control in smart grids.

Hao Liang (S'09–M'14) received the Ph.D. degree in electrical and computer engineering from the University of Waterloo, ON, Canada, in 2013. He is currently a Postdoctoral Research Fellow with the Broadband Communications Research Lab and Electricity Market Simulation and Optimization Lab with the University of Waterloo. His research interests are in the areas of smart grid, wireless communications, and wireless networking.

Dr. Liang was the System Administrator of IEEE TRANSACTIONS ON VEHICULAR TECHNOLOGY. He served as a Technical Program Committee (TPC) Member for major international conferences in both the information/communication system discipline and the power/energy system discipline, including IEEE International Conference on Communications (ICC), IEEE Global Communications Conference (Globecom), IEEE VTC, IEEE Innovative Smart Grid Technologies Conference (ISGT), and IEEE International Conference on Smart Grid Communications (SmartGridComm). He was a recipient of the Best Student Paper Award from the IEEE 72nd Vehicular Technology Conference (VTC Fall-2010), Ottawa, ON, Canada.

Ran Zhang received the B.E. degree in electronics engineering from Tsinghua University, Beijing, China, in 2010. He is currently working toward the Ph.D. degree in broadband communication research group with the University of Waterloo, Waterloo, ON, Canada. His current research interest includes resource management in heterogeneous wireless access networks, carrier aggregation in long-term evolution—advanced systems, and electrical vehicle charging control in smart grids.

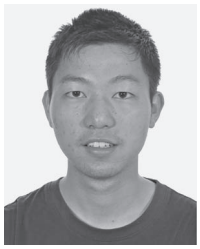

Ruilong Deng (S'11) received the B.Sc. degree in automation from Zhejiang University, Hangzhou, China, in 2009, when he also graduated from Chu Kochen Honors College. He is currently working toward the Ph.D. degree with the Department of Control Science and Engineering, and a Member of the Group of Networked Sensing and Control with the State Key Laboratory of Industrial Control Technology, Zhejiang University. He was a Visiting Student with Simula Research Laboratory in 2011, and the University of Waterloo from 2012 to 2013. His research interests are wireless (rechargeable) sensor networks, spectrum sensing in cognitive radio networks, and control and communication in smart grid. Mr. Deng served as a TPC Member for IEEE SmartGridComm'13 Demand Response Symposium and received a Student Travel Grant for IEEE GLOBECOM'13.

Xuemin (Sherman) Shen (M'97–SM'02–F'09) received the B.Sc. degree from Dalian Maritime University, Dalian, LiaoNing, China, in 1982 and the M.Sc. and Ph.D. degrees from Rutgers University, Camden, NJ, USA, in 1987 and 1990, all in electrical engineering. He is a Professor and University Research Chair with the Department of Electrical and Computer Engineering, University of Waterloo, Waterloo, ON, Canada. From 2004 to 2008, he was the Associate Chair for Graduate Studies. His research focuses on resource management in interconnected wireless/wired networks, wireless network security, wireless body area networks, vehicular *ad hoc* and sensor networks. He is a coauthor/editor of six books, and has published many papers and book chapters in wireless communications and networks, control and filtering. Dr. Shen served as the Technical Program Committee Chair for IEEE VTC'10 Fall, the Symposia Chair for IEEE ICC'10, the Tutorial Chair for IEEE VTC'11 Spring and IEEE ICC'08, the Technical Program Committee Chair for IEEE Globecom'07, the General Co-Chair for Chinacom'07 and QShine'06, the Chair for IEEE Communications Society Technical Committee on Wireless Communications, and P2P Communications and Networking. He also serves/served as the Editor-in-Chief for IEEE Network, Peer-to-Peer Networking and Application, and IET Communications; a Founding Area Editor for IEEE TRANSACTIONS ON WIRELESS COMMUNICATIONS; an Associate Editor for IEEE TRANSACTIONS ON VEHICULAR TECHNOLOGY, Computer Networks, and ACM/Wireless Networks; and the Guest Editor for IEEE JSAC, IEEE Wireless Communications, IEEE Communications Magazine, and ACM Mobile Networks and Applications. He is a registered Professional Engineer of Ontario, Canada, a Fellow of the Canadian Academy of Engineering, a Fellow of Engineering Institute of Canada, and a Distinguished Lecturer of IEEE Vehicular Technology Society and Communications Society.